The Astrophysical Journal, 718:502–512, 2010 July 20 doi:10.1088/0004-637X/718/1/502

THE EFFECT OF MAGNETIC ACTIVITY ON LOW-MASS STARS IN ECLIPSING BINARIES

Juan Carlos Morales[1], José Gallardo[2], Ignasi Ribas[1,3], Carme Jordi[1,4], Isabelle Baraffe[5,6], and Gilles Chabrier[5]
[1] Institut d'Estudis Espacials de Catalunya (IEEC), Edif. Nexus, C/ Gran Capità, 2-4, 08034 Barcelona, Spain; morales@ieec.uab.es
[2] Departamento de Astronomía, Universidad de Chile, Casilla 36-D, Santiago, Chile
[3] Institut de Ciències de l'Espai (CSIC-IEEC), Campus UAB, Facultat de Ciències, Torre C5 - parell - 2a planta, 08193 Bellaterra, Spain
[4] Departament d'Astronomia i Meteorologia, Institut de Ciències del Cosmos, Universitat de Barcelona, C/ Martí i Franquès 1, 08028 Barcelona, Spain
[5] École Normale Supérieure de Lyon, CRAL (UMR CNRS 5574), Université de Lyon, France
[6] School of Physics, University of Exeter, Stocker Rd, Exeter EX4 4QL, UK
Received 2010 February 10; accepted 2010 May 26; published 2010 July 1

ABSTRACT

In recent years, analyses of eclipsing binary systems have unveiled differences between the observed fundamental properties of low-mass stars and those predicted by stellar structure models. Particularly, radius and effective temperatures computed from models are ∼5%–10% lower and ∼3%–5% higher than observed, respectively. These discrepancies have been attributed to different factors, notably the high levels of magnetic activity present on these stars. In this paper, we test the effect of magnetic activity both on models and on the observational analysis of eclipsing binaries using a sample of such systems with accurate fundamental properties. Regarding stellar models, we have found that unrealistically high spot coverages need to be assumed to reproduce the observations. Tests considering metallicity effects and missing opacities on models indicate that these are not able to explain the radius discrepancies observed. With respect to the observations, we have tested the effect of several spot distributions on the light curve analysis. Our results show that spots cause systematic deviations on the stellar radii derived from light curve analysis when mainly distributed over the stellar poles. Assuming the existence of polar spots, overall agreement between models and observations is reached when ∼35% spot coverage is considered on stellar models. Such spot coverage induces a systematic deviation in the radius determination from the light curve analysis of ∼3% and is also compatible with the modulations observed on the light curves of these systems. Finally, we have found that the effect of activity or rotation on convective transport in partially radiative stars may also contribute to the explanation of the differences seen in some of the systems with shorter orbital periods.

Key words: binaries: eclipsing – binaries: spectroscopic – stars: activity – stars: evolution – stars: late-type – starspots

1. INTRODUCTION

Analyses of double-lined eclipsing binary stars (hereafter EBs) have provided fundamental properties of stars on the low-mass end of the Main Sequence. Such EB systems have been revealed to be the best candidates to test stellar structure models because they can potentially yield masses and radii for M-type stars with uncertainties below ∼1% (Morales et al. 2009b). However, results coming from a variety of independent studies indicate that differences exist between the observed properties and those predicted by models; for the same mass (M), models predict a ∼5%–10% smaller radius (R) and a ∼3%–5% larger effective temperature ($T_{\rm eff}$) than observed for stars below 1 $M_{\odot}$. In contrast, the stellar luminosity for these binary components is in agreement with those of single stars and also with theoretical models (see Ribas 2006, for a review).

Several authors have argued that activity could be the cause of discrepancies found between models and observations of these systems (Torres & Ribas 2002; López-Morales & Ribas 2005; Torres et al. 2006; López-Morales 2007; Ribas et al. 2008). Further support to this hypothesis is lent by similar radius discrepancies found when comparing single magnetically active late-type stars with their inactive counterparts (Morales et al. 2008), and by the results of interferometric observations of single inactive stars (Demory et al. 2009). Until now, all the known low-mass EBs are close binaries with periods well below 10 days, thus they are expected to be synchronized (Mazeh 2008), i.e., with their rotation tidally locked to the orbital motion, and therefore they are fast rotators ($v_{\rm rot} \gtrsim 10$ km s^{-1}). Such fast rotation in the presence of magnetic fields could trigger high levels of activity that may modify the structure of these stars in some respects. Observationally, the high activity of these stars is usually confirmed by saturated X-ray emission ($\log L_X/L_{\rm bol} \sim -3$), strong chromospheric emission in the Hα Balmer line, flares, and modulations on the light curves caused by the presence of starspots on the stellar surface.

Over the past decades, substantial progress toward the understanding of the structure and evolution of low-mass stars has been made, also including activity effects. Chabrier et al. (2007) showed that the introduction of rotation and/or magnetic field effects on the models of Baraffe et al. (1998) could explain the discrepancies between the observed and theoretically predicted mass–radius relationship of EBs. Specifically, they presented two scenarios considering: (1) that the effect of magnetic field and rotation alter the efficiency of convective energy transport, which can be modeled by setting the mixing length parameter (α from Mixing Length Theory) to lower values than those used for solar models; and (2) that the stellar magnetic activity present on these objects can be associated with the appearance of dark spots covering the radiative surface, which can be modeled by assuming a new stellar luminosity, $\hat{L} \propto (1-\beta)\,\hat{R}^2\hat{T}_{\rm eff}^4$, where $\hat{R}$ and $\hat{T}_{\rm eff}$ are the modified stellar radius and effective temperature, respectively, and β is the factor of spots blocking the outgoing luminosity due to their lower temperature (see Section 3 for further details on this parameter).

The results of Chabrier et al. (2007) show that both of these scenarios predict larger radius than standard stellar models, but while the effect of spots is significant over the entire

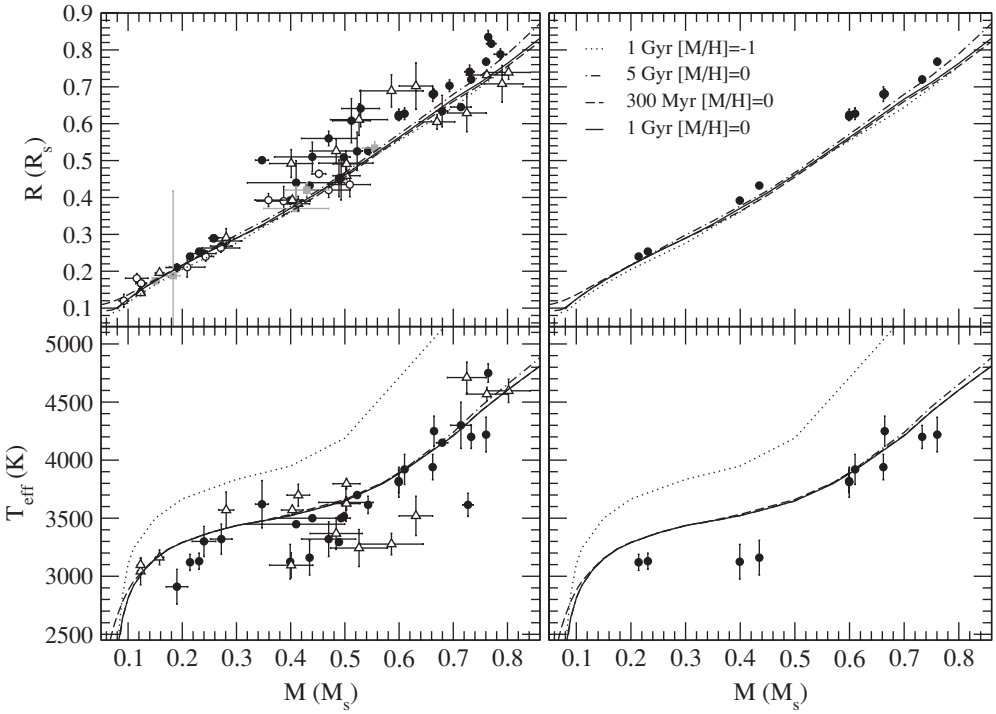

Figure 1. Different sets of theoretical M–R and M–$T_{\rm eff}$ relationships compared with observational values of low-mass stars. Left: low-mass stars in double-lined EB systems (filled circles), single-lined EB systems (open circles), M stars in post-common envelope binaries (gray squares), and late-type stars with radius measured interferometrically (open triangles). Right: same plots showing the EBs included in our analysis (see the text and Table 1). Theoretical models with different sets of parameters as labeled are from Baraffe et al. (1998).

low-mass domain, the effect of convection is relatively smaller for fully convective stars ($M \leqslant 0.4\,M_{\odot}$) because convection is nearly adiabatic and changing the mixing length parameter has a modest impact on their stellar structure. Since radius discrepancies have been reported over a wide range of masses, this may be indicating that either the contribution of spots or a combination of spots and activity effect on convective transport are needed to reconcile models with observations.

New accurate fundamental properties of low-mass EBs, and especially the case of CM Dra (Morales et al. 2009b), providing precise characterization of two fully convective stars, make it worthwhile to carry out a new thorough analysis of the agreement between observation and theory using the scenario suggested in Chabrier et al. (2007). In Section 2, we briefly describe the discrepancies between stellar structure models and current observations of low-mass stars and we select the sample of best-known EB systems to constrain stellar models. In Section 3, we analyze the effect of the photospheric spots on EB light curves and on the parameters fitted to these curves. Critical comparison with models including activity effects is discussed in Section 4, and finally, the conclusions are presented in Section 5.

2. LOW-MASS EBs COMPARED WITH MODELS

The properties describing the evolutionary phase of a star are its mass, chemical composition, and age. Given these three properties, radius and effective temperature are determined from stellar evolutionary models. Therefore, models could be tested by comparing the theoretical M–R and M–$T_{\rm eff}$ relationships with observational values. In Figure 1, such comparisons are shown for the models of Baraffe et al. (1998) and the full sample of low-mass stars with known physical properties. This figure includes properties derived from double-lined and single-lined EBs, interferometric radius measurements, and also from analysis of M-type stars in post-common envelope binaries, although some of these measurements are not independent of theoretical models or calibrations. In post-common-envelope components, the systems may not be reliable representations of the stars described by models due to interactions suffered during the common envelope phase.

In Figure 1, a clear difference between stars below and above $\sim$0.35 $M_{\odot}$ is apparent. On the lower end, radii are much closer to theoretical models and less scattered, while on the upper end, the scatter is larger and there seems to be a larger difference with models as well. This was already noticed in previous analyses (Ribas 2006) and it may be consistent with the boundary between fully convective stars ($M \lesssim 0.35\,M_{\odot}$) and partially radiative stars. Considering these two regimes, differences between all known measured radii of low-mass stars and the 1 Gyr solar metallicity model isochrone are 5.7% and 8.1% for fully convective and partially radiative stars, respectively. The dispersion of these differences is 3.1% and 12.2%, respectively, thus illustrating the scatter difference mentioned above. In the case of effective temperatures the differences are -1.9% and -1.6%, respectively, for this sample.

To test stellar structure models, masses and radii of stars need to be known with accuracies down to the few percent level (Andersen 1991; Torres et al. 2010). As mentioned earlier, EB systems provide the best opportunity to measure these fundamental stellar properties with such accuracy, as clearly visible in Figure 1. Thus, for our analysis we have selected all known low-mass stars with accuracies better than 3%. As reported recently by Torres et al. (2010), special attention should be paid to both the precision and the accuracy of the measures, and so we have excluded from our sample systems with error estimations that are not clearly described. Furthermore, we have only selected main-sequence systems with ages below 5 Gyr

Table 1
Properties of Observed EBs Included in Our Sample

EB	P (days)	M ($M_\odot$)	R ($R_\odot$)	$T_{\rm eff}$ (K)	[M/H]	Age Gyr	$v_{\rm rot,sync}$ (km s^{-1})	Ref.[a]
V818 Tau B	5.61	0.7605 ± 0.0062	0.768 ± 0.010	4220 ± 150	0.13	0.6	6.95 ± 0.09	1
IM Vir B	1.31	0.6644 ± 0.0048	0.681 ± 0.013	4250 ± 130	−0.28	2.4	26.12 ± 0.50	2
NGC2204-S892 A	0.45	0.733 ± 0.005	0.720 ± 0.010	4200 ± 100	...	...	80.9 ± 1.1	3
NGC2204-S892 B		0.662 ± 0.005	0.680 ± 0.020	3940 ± 110			76.4 ± 2.2	
GU Boo A	0.49	0.6101 ± 0.0064	0.627 ± 0.016	3920 ± 130	∼0	1.0	64.7 ± 1.6	4
GU Boo B		0.5995 ± 0.0064	0.624 ± 0.020	3810 ± 130			64.4 ± 1.6	
YY Gem A & B	0.81	0.5992 ± 0.0047	0.6194 ± 0.0057	3820 ± 100	∼0	0.4	38.88 ± 0.36	4
CU Cnc A[b]	2.77	0.4349 ± 0.0012	0.4323 ± 0.0055	3160 ± 150	∼0	0.32	8.02 ± 0.10	4
CU Cnc B[b]		0.3992 ± 0.0009	0.3916 ± 0.0094	3125 ± 150			7.30 ± 0.17	
CM Dra A	1.27	0.2310 ± 0.0009	0.2534 ± 0.0019	3130 ± 70	−1/−0.6	4.1	10.02 ± 0.08	4
CM Dra B		0.2141 ± 0.0008	0.2398 ± 0.0018	3120 ± 70			9.51 ± 0.07	

Notes.
[a] References: (1) Torres & Ribas 2002; (2) Morales et al. 2009a; (3) Rozyczka et al. 2009; (4) Torres et al. 2010.
[b] $T_{\rm eff}$ could be underestimated due to the presence of circumbinary dust.

and masses below 0.8 $M_\odot$ to restrict radius differences due to evolution below 2% and also to minimize the effect of mixing length differences between low-mass and solar mass models. The mechanical and thermal properties for each component of the selected systems are listed in Table 1, as well as the age and metallicity when known. Comparison of this sample with models is shown on the right panels of Figure 1. For the subsample of Table 1, the comparison with the 1 Gyr solar metallicity model gives discrepancies with observations of 5.8% and −6.1% in radii and effective temperatures, respectively, for fully convective stars (CM Dra), and 7.8% and −3.0%, respectively, for partially radiative stars.

Besides magnetic activity, several model parameters such as metallicity or opacities (Berger et al. 2006; Casagrande et al. 2008) have been proposed to explain the discrepancies between theory and observations. Our calculations indicate that metallicity produces differences between ∼4% and ∼20% on the radius and effective temperature values predicted by models, respectively, when comparing [M/H] = 0.0 and [M/H] = −1.0 models (solid and dashed line, respectively, in Figure 1). However, none of the systems are known to have such low metallicity, except for the case of CM Dra, for which its metallicity is not well established, and NGC2204-S892, for which there is no determination. Besides, radius differences are lower than needed to reproduce observations even with metallicities as low as [M/H] = −1.0. Therefore, metallicity effects are not expected to be significant in our sample. In the case of effective temperature comparisons, where the effect of metallicity is more important, EB light curves only provide accurate values of the temperature ratio for the components. The individual effective temperatures are usually computed using different spectrophotometric calibrations for each system, thus introducing the potential for systematic errors. Furthermore, some EB systems may have peculiarities, such as CU Cnc, which is supposed to have a circumbinary dust disk that may affect the temperature determination. Thus, to investigate the agreement between models and observations we will primarily make use of the M–R relationship, as both fundamentally determined quantities.

Recently, the possibility of underestimated opacities has been raised in the context of the Standard Solar Model. An increase of opacities near the bottom of the convective zone has been shown to reconcile helioseismic data of the Sun with models using the new chemical composition (Bahcall et al. 2004, 2005). These results, as well as others found in the literature invoking problems with the atmospheric opacities as a source of the discrepancies present in observed radii of EB compared with theoretical models, prompted us to perform different tests to analyze the effect of atmospheric opacity on the resulting stellar radius. Using the standard Lyon group stellar evolutionary models (Baraffe et al. 1998), an overall massive increase by a factor of ∼10 in the opacity affects the radius by just 4% (and even this difference is smaller below the fully convective boundary), as already shown by Chabrier & Baraffe (1997). To obtain a ∼10% larger radius, the opacities of eclipsing binaries would have to be increased to unrealistically high values. Missing elemental opacities do not seem to be enough to explain the ∼5%–10% radius disagreement between models and observations. Moreover, both metallicity and opacity effects should also be present on single stars, which are known to be well described by models, as recently confirmed by Demory et al. (2009) from the comparison of interferometric radius measurements of inactive low-mass stars with model predictions. Further, the authors did not find a correlation between metallicity and radius differences, and thus did not confirm the results from Berger et al. (2006). Further, similar radius differences as those reported here are known between single magnetically active stars and their inactive counterparts (Morales et al. 2008), thus strengthening the activity hypothesis.

3. DETERMINATION OF PHYSICAL PROPERTIES OF EBs

The conclusions of the previous section reinforce magnetic activity as the most reasonable explanation for the discrepancies found between stellar models and observations of low-mass stars. Before embarking on a careful fine-tuning of model parameters to reach agreement with observations, it is worth evaluating whether our observed eclipsing binary parameters could be affected by the strong magnetic activity of the components. Time-variable brightness changes are a common signature of the presence of activity on low-mass stars both on single and eclipsing binaries. In the latter case, the modulation present on the light curves is combined with the eclipsing variability and, therefore, starspots must be taken into account to derive accurate stellar fundamental properties. In this section, we study the possibility that starspots could be responsible for systematic

effects inherent to the light curve and radial velocity analyses in the case of the very active low-mass eclipsing binaries. We analyze whether the fundamental properties determined from the classical modeling could be biased because of the presence of starspots in different geometries.

Absolute physical properties of EBs are obtained from the combination of the results of light and radial velocity curve analyses with modeling codes such as the widely used Wilson–Devinney (hereafter WD; Wilson & Devinney 1971). Light curves yield properties such as the inclination of the orbit (i), the ratio of effective temperatures ($T_{\rm eff\,2}/T_{\rm eff\,1}$), the luminosity ratio in the light curve bandpass (L_2/L_1), and the surface potentials (Ω_1 and Ω_2), which are related to the radii relative to the semimajor axis (r_1 and r_2). Radial velocity curves provide values for the mass ratio (q) and projected semimajor axis ($a \sin i$). The combination of the two modeling procedures yields the absolute properties of the components independent of models or distance calibrations. Radiative parameters, such as limb darkening and gravity darkening, relevant for light curve analyses, are usually taken from theory.

The presence of spots on the surface of the components of an EB system causes perturbations on both the light and radial velocity curves. The most prominent effect is on light curves, in which modulations in the out-of-eclipse phases appear due to the transit and occultation of spots according to the orbital and spin motions. To appropriately derive physical properties of the components, the spot effect must be taken into account when analyzing these curves. The WD code introduces spots on the modeling assuming that they are circular and that they have a uniform temperature ratio with respect to the photosphere. With this simple model, properties of spots, such as their location in co-latitude (θ_s, measured from north pole) and longitude (ϕ_s), the angular size (r_s), and the temperature contrast with the photosphere, i.e., $\frac{T_{\rm eff,s}}{T_{\rm eff}}$, where $T_{\rm eff}$ and $T_{\rm eff,s}$ are the effective temperatures of the photosphere and the spots, respectively, can be fitted. The values of $\phi_{\rm s}$ and $r_{\rm s}$ are well constrained by the central phase of the modulation and its duration and amplitude, respectively, however the amplitude is also dependent on $\theta_{\rm s}$ and $\frac{T_{\rm eff,s}}{T_{\rm eff}}$, so these parameters are strongly correlated with the size of spots. This model can reproduce the presence of complex and irregular spot groups by equivalent circular spots with an average temperature.

The total luminosity of a spotted star is the addition of the contribution of the spots at an effective temperature $T_{\rm eff,s}$ and the immaculate surface at $T_{\rm eff}$. If we consider S and $S_{\rm s}$ to be the surface of the star and that covered by spots, respectively, the total luminosity is given by

$$L = (S - S_{\rm s})\sigma {T_{\rm eff}}^4 + S_{\rm s}\sigma {T_{\rm eff,s}}^4. \quad (1)$$

Comparing this equation with the formalism introduced by Chabrier et al. (2007), it can be concluded that the β parameter is given by

$$\beta = \frac{S_{\rm s}}{S}\left[1 - \left(\frac{T_{\rm eff,s}}{T_{\rm eff}}\right)^4\right]. \quad (2)$$

This equation indicates that the β parameter is related with the properties of spots. For completely dark spots ($T_{\rm eff,s} = 0$), the term in brackets in Equation (2) is exactly one, therefore, β is a measure of the fraction of stellar surface covered by dark spots as defined by Chabrier et al. (2007). However, in the realistic case that spots are not completely dark, the term in brackets is less than one and β is lower than the fraction of spotted surface. For a given $T_{\rm eff}$ and an estimation of the contrast of spots, Equation (2) provides the fraction of the surface covered by spots when β is known, or vice versa.

Spot modeling results have been published for several of the best-known EBs (Torres & Ribas 2002; Ribas 2003; López-Morales & Ribas 2005; Morales et al. 2009a, 2009b) reporting both cold and hot spots with radii between ∼9 deg and ∼90 deg and with temperature factors ($T_{\rm eff,s}/T_{\rm eff}$) down to 0.86. Hot spots can be interpreted as photospheric regions surrounded by large cool spots. Considering the spot parameters given in the above references for the cases of IM Vir, GU Boo, YY Gem, CU Cnc, and CM Dra, we find β values of up to 0.1 according to Equation (2). This value is much smaller than the range between 0.3 and 0.5 suggested by Chabrier et al. (2007). It must be mentioned, though, that since the relevant measures in EB light curve analyses are differential magnitudes, the photometric variations used to derive the spot parameters are not sensitive to the total surface covered by spots but to the contrast between areas with different effective temperatures. For instance, an evenly spotted star would not show significant light curve variations. It is thus possible that EBs could be more heavily spotted than simple photometric variations indicate and permit β values higher than 0.1. A check of the photometric variations that could produce such higher values of β and their effect on derived parameters from fits are described in the following sections.

3.1. Modulation on Light Curves

For M-type stars, an assumption of $T_{\rm eff} \sim 3500$ K and spots about ∼500 K cooler than the photosphere and β values between 0.3 and 0.5 corresponds to a fractional surface area of 65%–100% covered by spots (as shown by Equation (2)). To test the consistency between the theoretical modulations expected from different β values and the spot modulations observed on EB light curves, we simulated EB systems with components randomly spotted and used the WD code to generate their light curves. Such theoretical light curves were subsequently compared with those observed in EBs.

We have developed a code to randomly place spots on the surface of stars. We assumed a uniform longitude distribution and tried different distributions over latitude. Granzer et al. (2000) calculate the probability of spot appearance for different latitudes as a function of spin period and mass. Their results show that for a star like the components of GU Boo (see Table 1), spots are formed in a band from 25 deg to 55 deg of co-latitude. Both bands (one per hemisphere) represent about one-third of the stellar surface, which is not enough to simulate spot coverages with β greater than 0.15 (assuming spots 500 K cooler than the photosphere). Doppler tomography analyses have revealed the prominent existence of polar spots on active stars (Jeffers et al. 2007; Washuettl & Strassmeier 2001; see also Strassmeier 2009, and references therein). Thus, we decided to extend the distribution to all stellar latitudes. To use similar distributions as those given in Granzer et al. (2000), we considered a linear probability from the pole to 40 deg and from 45 deg to the equator with a plateau between 45 deg and 40 deg (hereafter Distribution 1). This roughly mimics distributions of 0.6 $M_\odot$ rapidly rotating stars. For comparison, we also considered a bilinear distribution from the pole to 70 deg with a peak at 25 deg. This is similar to the 0.4 $M_\odot$ distribution in Granzer et al. (2000) for rapidly rotating stars but extended to cover β factors up to 0.3 (hereafter Distribution 2). Finally, we considered a completely uniform distribution.

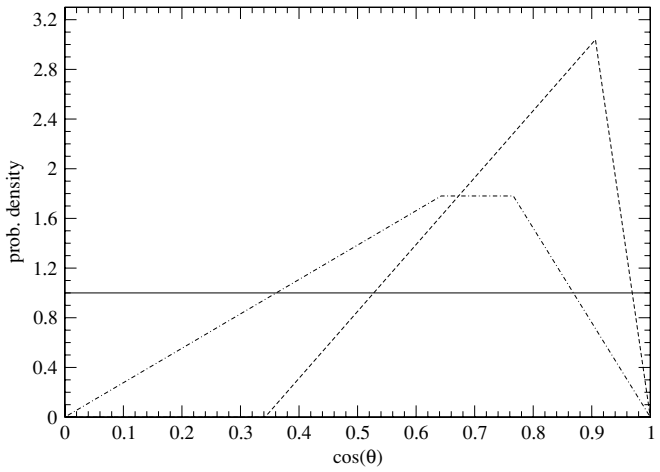

Figure 2. Probability density functions over $\cos\theta$ used to simulate spotted stars. The equator corresponds to $\theta = 90°$. The uniform distribution (solid line), Distribution 1 (dot-dashed line), and Distribution 2 (dashed line) are described in the text.

These distributions are shown in Figure 2 and it illustrates that Distribution 2 is more concentrated toward the poles. Additionally, to have reasonable computing time using the WD code, we limited the number of spots by imposing that the centers of two spots could not be closer than half their radius, i.e., each spot contributes at least ∼30% of its surface to the total spot coverage.

The simulation procedure was executed as follows. We considered spots with a temperature contrast with the photosphere of 0.85, even on overlapping areas (i.e., the temperature contrast in the area where two spots overlap is also 0.85). This value constrains β between 0 and ∼0.5, the latter meaning a completely spotted stellar surface. In the case of Distribution 2, the upper value of β is ∼0.35. We chose 10 deg as spot radius in line with large spot groups measured on the Sun. Then, for each latitude distribution we simulated 25 light curves with spots randomly distributed over the surface of the components for different values of β. From these simulated light curves, we measured the peak-to-peak variations on the out-of-eclipse phases and computed the mean value of the 25 light curves. This procedure was done using the physical properties of GU Boo as a template and using *R*-band light curves. However, since the effect of absolute masses or mass ratio on the light curves is negligible, this should be representative of the entire low-mass star domain.

The values of the peak-to-peak modulations found with these simulations were later compared with the real values for the best-known EBs. Figure 3 shows the peak-to-peak modulations resulting from simulations for each distribution compared with a few observational values as reference. Large modulations are better explained by mild spot coverages assuming a uniform distribution or Distribution 1, while low spot signals are better reproduced by Distribution 2. However, the amplitude of these modulations depends on the size and thermal properties of the spots as shown in Figure 4. It is clear that the observed modulations could be explained with any of the distributions when considering the different spot sizes and the intrinsic dispersion of the modulation. Therefore, low amplitudes such as those of YY Gem and CM Dra could be recovered with a mild spot coverage with small size or low temperature contrast spots. Besides, the variability of the spot properties should also be taken into account since it could induce different modulations on different epochs as has been reported for the case of *V*-band

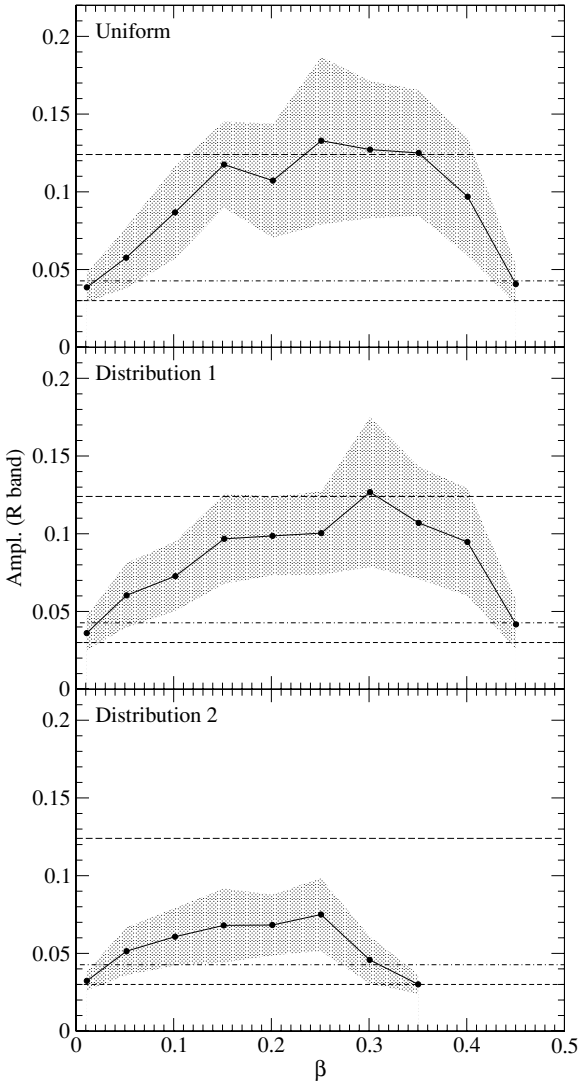

Figure 3. Amplitude of the modulations produced by different β spot scenarios using different spot distributions on *R*-band light curves. Each point is the mean value of 25 realizations and the shaded area shows the standard deviation of these modulations. The values reported in the literature for CM Dra (dashed line), YY Gem (dot-dashed line), and GU Boo (long-dashed line) are shown for comparison.

light curves of YY Gem, showing amplitudes of 0.09 mag and 0.055 mag in different seasons (Torres & Ribas 2002).

Several other distributions, such as linear, quadratic, and square root from equator to poles were tested yielding results between the uniform and Distribution 1 cases.

3.2. Systematics on Light Curves Due to Spots

The simulations described above were also used to investigate systematic effects of spots on fits to light curves. A thorough statistical analysis of the systematic deviations induced by the presence of spots on these parameters would require fitting all the simulated light curves by treating them as real observations. Typical light curve analyses involve testing fits for different parameters, especially when spots are present, since different spot configurations should be tested. Simultaneous fits of light curve in several bands are also preferable in order to avoid correlations between parameters such as limb darkening and radius. Besides, spot parameters are degenerate and thus the inversion of a light curve to recover the input parameters is an ill-posed

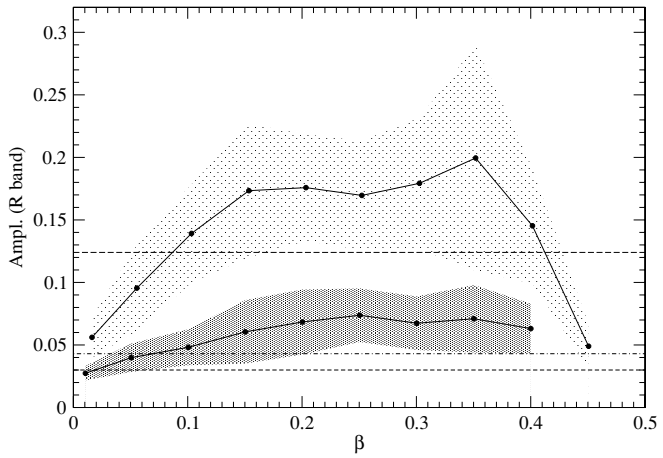

Figure 4. Same as Figure 3 for the uniform distribution comparing the cases of simulations using spots with radius of 15 deg (light shade) and 5 deg (dark shade).

problem. This implies carrying out a slow procedure consisting in adding spots and evaluating the relevance of the modulation to reach the best compromise between stability and the quality of the fit to the observations. For these reasons, fitting all the simulated curves is prohibitively time consuming. We performed fits to three simulated light curves for each distribution and for each of the β values 0.1, 0.2, 0.3, and 0.4 (33 light curves in total) with the aim of inferring a general trend. Besides, we focused our attention on the R band to reduce the computing time. This band is commonly used in the photometric follow-up of low-mass eclipsing binaries and it is thus representative of light curve analyses. A possible bias resulting from the correlation between radius and limb darkening coefficients should be negligible because the coefficients are computed from the same theoretical tables (Claret 2000) both for simulations and fits. For each of the β values mentioned, we chose as representative spotted light curves three realizations with modulation amplitudes representative of the average.

We added random Gaussian noise of 1% of the flux to the simulations so that the typical scatter of light curves is reproduced. We subsequently performed fits with the WD code. Light curve-relevant parameters such as the inclination, temperature ratio, light ratio, and surface potentials were fitted along with spot properties. Since some of the spot parameters are highly correlated, we started assuming spots at 45 deg latitude and 10% cooler or hotter than the photosphere. The free parameters were the longitude (ϕ_s) and size (r_s) of spots and, in a second step, the latitude (θ_s) and temperature contrast ($T_{\rm eff,s}/T_{\rm eff}$). As the usual practice, we included in the model as many spots as needed to obtain a realistic fit and we tested the location of spots on primary component, secondary or both at the same time. All cases yielded satisfactory fits with 1–3 spots on different components. We found best fits with $T_{\rm eff,s}/T_{\rm eff}$ ratios of $\sim$0.9, thus indicating that spot groups could be modeled with a smoother temperature contrast than real. A phase shift was also set as a free parameter to account for phase corrections due to spots.

Figure 5 depicts two examples of the fits together with the configuration of the simulated spots on the stars, and Figure 6 shows all the 33 fits performed. In Figure 7, we illustrate the effect of spots on the radius, both by plotting the mean values and standard deviations (error bars) of the systematic differences with respect to the input values of the simulations. The sum and

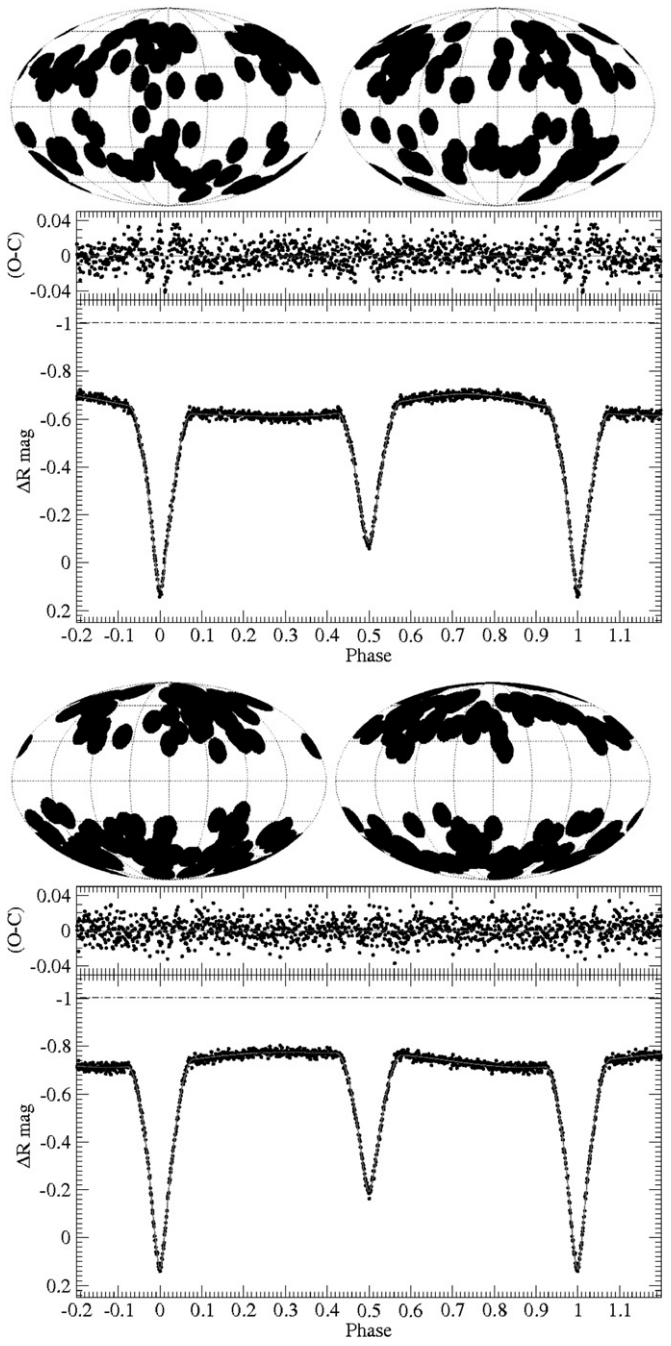

Figure 5. Two representations (top panel for Distribution 1 and bottom panel for Distribution 2) of simulated spotted EB systems (primary component on the left and secondary on the right) with the resulting light curves. Star surfaces are represented in a Mollweide projection and the center of each one corresponds to 0 deg of longitude and 90 deg of co-latitude (equator). Best fits to the simulated light curves together with the O–C residuals are shown. Both cases were simulated with $\beta = 0.2$. The reference level of the unspotted light is shown for comparison (dot-dashed line).

the ratio of radii relative to the semimajor axis were used to check for systematic effects since these are the parameters that directly depend on the shape of the eclipses. A clear trend is seen in the case of Distribution 2, where the sum of the radii of the components (i.e., total size of the stars) is systematically overestimated by the fits by 2%–6%. For distributions less concentrated to the pole, the deviations induced by spots seem to be random. In the case of the ratio of radii, the differences found do not seem to be significant in any of the cases, especially

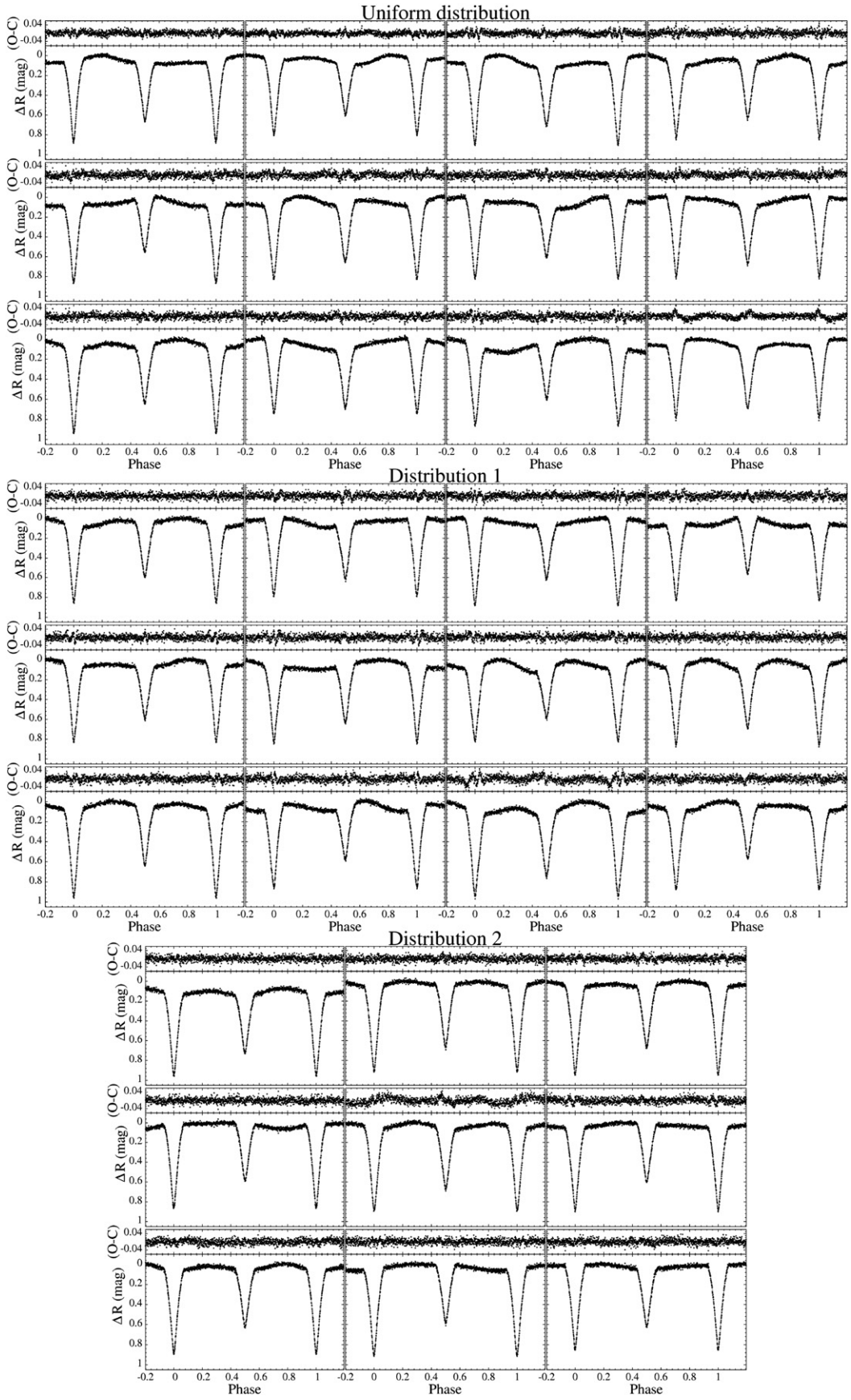

Figure 6. Fits to simulated light curves following the procedure explained in the text. Light curves are vertically shifted to be plotted with the same scale. Each block corresponds to a different spot distribution as indicated. Simulations with equal β value are arranged in columns, starting from $\beta = 0.1$ to 0.4 in steps of 0.1, except for Distribution 2, for which the last column corresponds to $\beta = 0.3$.

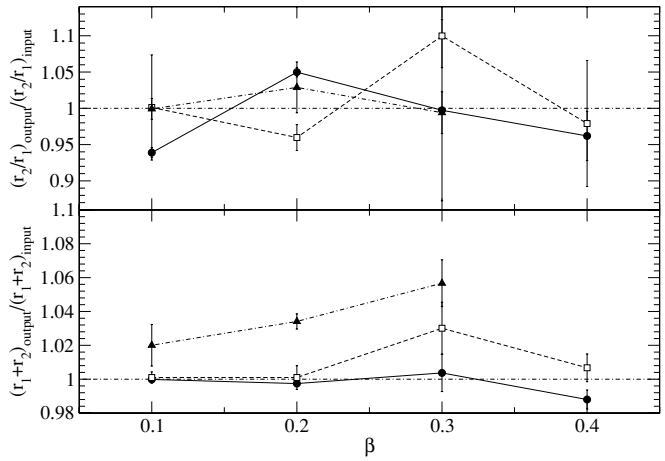

Figure 7. Differentials between input parameters to the simulations and those recovered from fits. The ratio and the sum of the radii are shown on the top and bottom panels, respectively, for different distributions: uniform (filled circles), Distribution 1 (open squares), and Distribution 2 (filled triangles). These values are computed as the average of the results of fits on three simulated light curves for each distribution. Standard deviations are shown as error bars.

when considering the dispersion. The same lack of systematic trends is found for other fit parameters such as the inclination, effective temperature ratio, or light ratio.

The parameters related to radial velocity curves, such as semimajor axis, mass ratio, and systemic radial velocity, were also inspected for deviations by simulating the corresponding velocity curves. Fits using the WD code were performed by ignoring the presence of spots and yielded insignificant differences in the mass ratio and semimajor axis, in all cases below 1% and 0.5%, respectively. As a consequence, the absolute radius derived for each component of the eclipsing binary system is not biased because of the effect of spots on the semimajor axis, which ultimately defines the scale of the system.

The systematically larger radii found from the distributions with polar spots have a relatively straightforward geometric interpretation. A projected star that has a polar cap loses its circular symmetry and its isophotes become elongated. This causes the eclipses to widen and the WD code, which assumes a Roche geometry (i.e., nearly spherical stars for these well-separated systems), finds a best fit with a larger stellar radius. In the case of spots more uniformly distributed in latitude, eclipses are not significantly affected, thus, systematic deviations appear more random. We tested this by assuming systems with pure polar caps (i.e., circular and symmetric dark spots covering both caps) and carrying out fits without considering the presence of spots (since no modulations are seen). The results confirm the existence of the systematic effect on the stellar radii found in the simulations with Distribution 2. Also, because of the much faster fits, we could test several input parameters (corresponding to the systems IM Vir, GU Boo, YY Gem, CU Cnc, and CM Dra) that yielded comparable results, thus testing the systematic effect on radius also for different values of relevant binary parameters such as inclination, relative radius, and temperature ratio. Using these simulations we also tested the influence of the photometric band by producing light curves in the *BVRIJK* filters. We found that the systematic effect on the radius is expectedly smaller in the near-IR bands because the spot contrast is lower. The radius differences range from ∼3.5% in *B* to ∼1.2% in *K*. The simultaneous fit of several bands still yields systematic radius differences, corresponding to some average of those resulting from fits to the individual filter light curves.

The outcome of this battery of tests is that the presence of starspots on the stellar surface could bias the determination of stellar radii. This is the case when spots are concentrated toward the poles. Doppler tomography imaging has revealed a pre-eminence of polar spots on rapidly rotating low-mass stars, such as AG Dor, AB Dor, and LO Peg (see Strassmeier 2009, for a review). YY Gem is the only EB system from our sample with published Doppler images (Hatzes 1995), although no indication of a polar cap was found. However, polar spots are difficult to detect with Doppler tomography for near edge-on inclinations, such as the case of YY Gem. Spectropolarimetric analyses of low-mass stars showing intense poloidal magnetic fields (see Donati & Landstreet 2009, for a review) may provide further evidence of polar spots. If polar caps are present in low-mass EBs, these could be responsible for up to ∼6% (if $\beta = 0.3$) of the radius discrepancy between models and observations. Thus, stellar models should be compared with observed values corrected from the systematic effect due to polar spots.

4. MODELING ACTIVE STARS

As already mentioned in Section 1, Chabrier et al. (2007) introduced activity effects in low-mass stellar models by considering two parameters: the spot blocking factor (β) and the modification of the mixing length parameter (α). The study of Chabrier et al. (2007) shows that the effects of the β and α parameters are degenerate; i.e., the properties of any given system can be reproduced by modifying any of the two or both, although for completely convective stars, the effect of reducing the mixing length parameter is very small.

CM Dra offers the possibility of discerning between the effects of activity on the convective efficiency (parameterized by α) and on surface spots (parameterized by β). This is because the components of this system should be fully convective and their structure almost independent of the mixing length parameter α. Thus, we used this system to find the β value that yields the best fit to the properties of the components of CM Dra. We compared the theoretical M–R relationships, interpolating between models with different β. To do so, we assumed the presence of polar spots on the components (see Section 3.2). Different negative corrections to the radii of the components were used depending on the value of β and in consistency with our simulations in Figure 7. An iterative process was employed until reaching agreement between the resulting β value and the radius correction from light curve systematics. After iterating, we find that a model with $\beta = 0.17 \pm 0.03$ reproduces both components when their radii are downward corrected by ∼3%. If spots are ∼15% cooler than the photosphere, the resulting β translates into (36 ± 6)% of the star surface covered by spots, a value that is in agreement with findings from Doppler imaging for other systems such as HK Aqr (Barnes & Collier Cameron 2001). Note, however, that spot coverages from Doppler tomography represent a lower limit because of the limited sensitivity of the technique to small-sized spots or low contrast temperatures.

Abundant X-ray observations have revealed a clear relation between magnetic activity and rotation, indicating that rapidly rotating stars are more active than slower rotators up to a certain limit where saturation is reached. Pizzolato et al. (2003) showed that M-dwarfs with rotation periods below ∼10 days show saturation of their X-ray emission, therefore we could assume that binaries in our sample are all in this regime of saturated

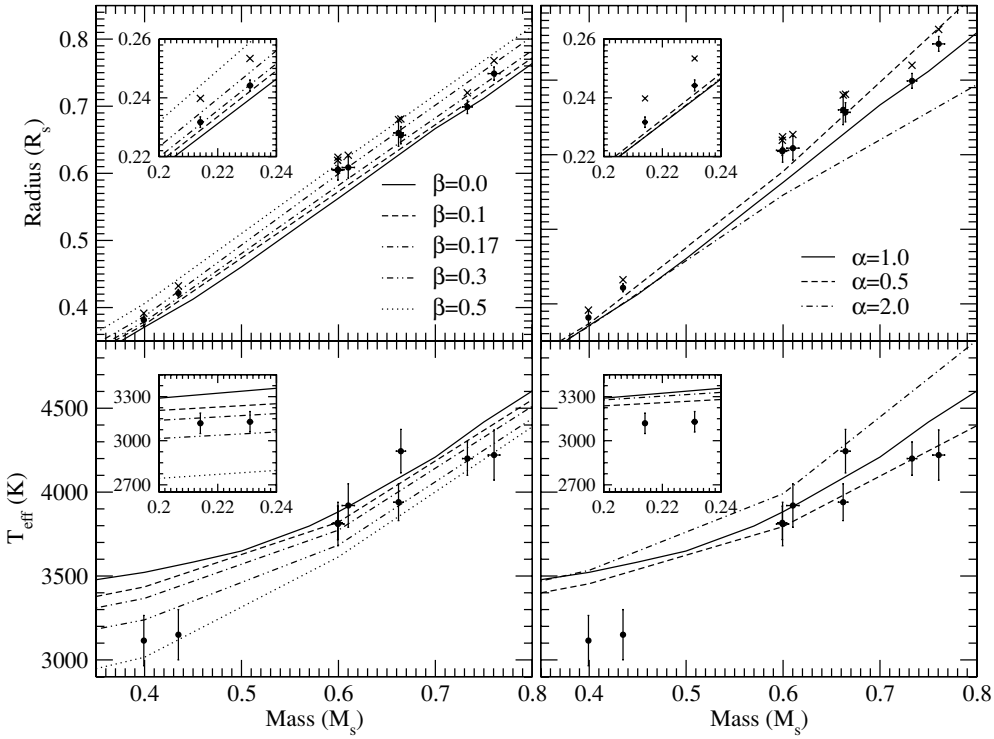

Figure 8. Comparison between models and observations for different β values and $\alpha = 1$ (left) and for different α values and $\beta = 0$ (right). Top panel: M–R relationship. Crosses indicate the measured radius of the EB components reported in Table 1, and circles represent the values corrected for the 3% systematic factor described in the text and further normalized to an age of 1 Gyr. Bottom: M–$T_{\rm eff}$ relationship. Circles represent temperature values normalized to an age of 1 Gyr. The insets display the case of CM Dra.

coronal activity. The physical mechanism of saturation is not well understood yet, but one of the feasible explanations could be that saturation is reached when the entire stellar corona is full of active regions. This may imply that the β parameter is similar for stars that are in the saturated regime.

At this point, we make two assumptions to proceed with the analysis: (1) that spots on active EBs are mostly polar and (2) that saturated systems have similar spot coverages (i.e., β is roughly independent of mass for very active systems). With these assumptions and following the same procedure applied above for CM Dra, we find that the overall sample of EB systems is reproduced within 1σ of their error bars with $\beta = 0.20 \pm 0.04$, i.e., $(42 \pm 8)\%$ of spot coverage.

The left panel of Figure 8 shows a comparison of mass and radius observations with models assuming different β values. The radii of the EB systems shown in the figure were corrected considering two effects: first, a 3% systematic difference resulting from the light curve analysis and second, an age effect on the stellar radii to put all systems at a normalized age of 1 Gyr (ages in Table 1, except for NGC2204-S892 where no age is available and no correction was made) using the models of Baraffe et al. (1998). The evolutionary radius offsets are always well below the 1% level. This allowed us to plot Figure 8 and compare all EBs with a theoretical model with the same age.

To serve as a reference, if we relax the polar spot assumption, i.e., we do not correct for the systematic effect of polar spots on light curves, the best model reproducing CM Dra gives $\beta = 0.37 \pm 0.04$, which means more than 75% of the surface of each component covered by spots. This seems to be a rather high value of spot coverage when compared with the results of Doppler imaging. If we do not consider the saturation hypothesis and assume that each system could be reproduced by different β factors, we find in systems such as YY Gem or GU Boo over half of the surface must be spotted. Note that the spot coverage estimates depend on the spot contrast, which is set to ∼500 K in this work.

Some remaining radius differences are still apparent in Figure 8 when considering a β value of 0.17. Systems such as YY Gem or GU Boo have observed radii well over 1σ of the model predictions. It is interesting to note that these are the systems with the fastest rotational velocity, which could be an indication of additional effects of rotation and/or magnetic activity not accounted for in the β analysis. The right panel of Figure 8 shows that for the more massive M-type EBs ($<0.6\,M_{\odot}$), the additional differences could be explained by reducing the mixing length parameter α. Figure 9 depicts the differences between the $\beta = 0.17$ model and observations (after correction for polar spots and normalized to 1 Gyr) as a function of the rotational velocity of each star (computed assuming synchronization). Although not significant, a general trend of increasing differences for increasing rotational velocities seems to be present. The exception is NGC2204-S892 (two rightmost points on the plot), which is the shortest period binary. But note that no determination of the age and metallicity of this EB system is available and this could be falsifying the analysis. The tentative trend may indicate that, while the spot effect (via the β parameter) is a clear contributor to explain the differences between observation and theory, the loss of efficiency of convective energy transport (related with magnetic fields and thus possibly with rotation rate) may also be at play, explaining up to 4% of the radius difference.

As stated in Section 2, absolute effective temperatures of EB components were not used to constrain model parameters because they are not determined independently of calibrations

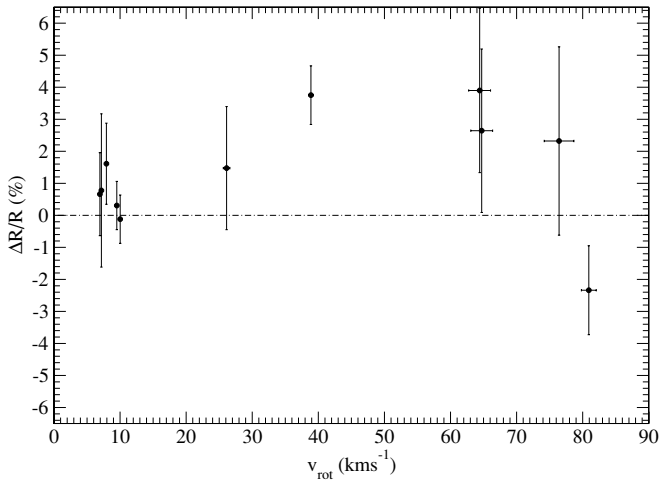

Figure 9. Residual discrepancy between observations and the model with $\beta = 0.17$ that best fits the case of CM Dra, which is not affected by variations of the mixing length parameter α.

as masses and radii. Nevertheless, we checked the consistency of the spot scenario with temperatures. The bottom panels of Figure 8 show the comparison between models and observations in the M–$T_{\rm eff}$ plane for different α and β values. The temperatures represented on these plots have been also normalized to an age of 1 Gyr using the models of Baraffe et al. (1998) although differences amount for less than 10 K in all cases. The model with $\beta = 0.17$ also reproduces the M–$T_{\rm eff}$ relationship of EBs within the errors, with the exceptions of IM Vir, possibly due to its subsolar metallicity, and CU Cnc, whose temperatures may be affected by a circumstellar dust disk. These figures also show that both models with lower α and the model with $\beta = 0.17$ reproduce all systems but CM Dra due to the negligible effect of mixing length on completely convective stars. Thus, the conclusions from the M–R analysis are also consistent with the effective temperature comparison.

5. CONCLUSIONS

After evaluating different scenarios to explain the discrepancies reported between observation and theory for low-mass stars, a rather complex picture is now emerging since no single effect can account for the full size of the differences. Our analysis shows that the ∼5%–10% radius discrepancy in M-type EBs is explained by combining three factors: (1) a systematic overestimation of the stellar radius in EB light curve analysis caused by the presence of polar spots with the subsequent loss of circular symmetry (amounting to about ∼3%); (2) an increase of stellar radii to compensate for the loss of radiative efficiency because of starspots (reproduced by models considering a β parameter of 0.17 that explains 2% of the radius difference); and (3) an increase of the radius caused by the lower convective efficiency in fast rotators with supposedly strong magnetic fields (reproduced by models through changing the α parameter) and accounting for 0%–4% of the radius difference. This scenario also reproduces the M–$T_{\rm eff}$ distribution of EBs although effective temperatures are not as fundamentally determined as radii.

Our overall analysis ensures self consistency by comparing with the constraints set by the observations. Predicted spot coverages and simulated light curves are found to reproduce the modulation amplitudes in the real light curves of the EB systems. Also, the ∼35% surface coverage is found to be compatible with results from Doppler tomography of active stars. Even relatively inactive systems such as some hosts of transiting exoplanets are found to have significant spot coverages when applying transit mapping procedures (Pont et al. 2007; Silva-Valio 2008).

It is important to note that our results are based on two main hypotheses: (1) that *all* of these active EB components have spots that preferentially occupy locations close to the pole (with consequent effect on the light curve analysis) in line with results from Doppler imaging; and (2) that *all* EB components have similar surface spottedness caused by their saturated activity regime. The first hypothesis relaxes the classical discrepancy with models to a lower 2%–7%, and the second hypothesis ensures that β will roughly be "universal" for these strongly active systems. In this framework, the system CM Dra is key to reaching the conclusions above. This is because it allows us to separate the effects of the two free parameters, namely β and α, since the components of this system are expected to be fully convective and little affected by changes in the mixing length parameter.

The analysis of low-mass stellar evolution models clearly shows that activity plays an important role on the structure of stars, and that when considering activity effects on stellar structure, models can reproduce the observed values of radii and effective temperatures of low-mass stars. Accurate masses and radii of new low-mass systems coming from missions such as *CoRoT* and *Kepler* should improve the statistics and better define the scenario proposed above, especially if comparable active and non-active EB systems are found. Doppler imaging of the EBs analyzed or new methods of mapping stars using interferometry (Monnier et al. 2007) should also give indications of the spot distribution on the stellar surfaces. All these efforts are valuable to understand the vast majority of the stars that populate the Galaxy and, notably, have an impact in the area of exoplanet research, in which planet properties are directly linked to our knowledge of the host star.

We are grateful to J. F. Donati for useful discussions and to the referee for helpful suggestions. J.C.M., I.R., and C.J. acknowledge support from the Spanish Ministerio de Ciencia e Innovación via grants AYA2006-15623-C02-01, AYA2006-15623-C02-02, AYA2009-06934, and AYA2009-14648-C02-01. This work was partly supported by the French ANR "Magnetic Protostars and Planets" (MAPP) project and by the "Programme National de Physique Stellaire" (PNPS).

REFERENCES

Andersen, J. 1991, A&AR, 3, 91
Bahcall, J. N., Basu, S., Pinsonneault, M., & Serenelli, A. M. 2005, ApJ, 618, 1049
Bahcall, J. N., Serenelli, A. M., & Pinsonneault, M. 2004, ApJ, 614, 464
Baraffe, I., Chabrier, G., Allard, F., & Hauschildt, P. H. 1998, A&A, 337, 403
Barnes, J. R., & Collier Cameron, A. 2001, MNRAS, 326, 950
Berger, D. H., et al. 2006, ApJ, 644, 475
Casagrande, L., Flynn, C., & Bessell, M. 2008, MNRAS, 389, 585
Chabrier, G., & Baraffe, I. 1997, A&A, 327, 1039
Chabrier, G., Gallardo, J., & Baraffe, I. 2007, A&A, 472L, 17
Claret, A. 2000, A&A, 363, 1081
Demory, B.-O., et al. 2009, A&A, 505, 205
Donati, J.-F., & Landstreet, J. D. 2009, ARA&A, 47, 333
Granzer, T., Schüssler, M., Caligari, P., & Strassmeier, K. G. 2000, A&A, 355, 1087
Hatzes, A. P. 1995, in IAU Symp. 176, Doppler Images of the dMe Binary YY Gem, ed. Klaus G. Strassmeier (Cambridge: Cambridge Univ. Press), 90
Jeffers, S. V., Donati, J. F., & Collier Cameron, A. 2007, MNRAS, 375, 567
López-Morales, M. 2007, ApJ, 660, 732
López-Morales, M., & Ribas, I. 2005, ApJ, 631, 1120

Mazeh, T. 2008, EAS Publ. Ser., 29, 1
Monnier, J. D., et al. 2007, Science, 317, 342
Morales, J. C., Ribas, I., & Jordi, C. 2008, A&A, 478, 507
Morales, J. C., Torres, G., Marschall, L. A., & Brehm, W. 2009a, ApJ, 707, 671
Morales, J. C., et al. 2009b, ApJ, 691, 1400
Pizzolato, N., Maggio, A., Micela, G., Sciortino, S., & Ventura, P. 2003, A&A, 397, 147
Pont, F., et al. 2007, A&A, 476, 1347
Ribas, I. 2003, A&A, 398, 239
Ribas, I. 2006, in ASP Conf. Ser. 349, Astrophysics of Variable Stars, ed. C. Sterken & C. Aerts (San Francisco, CA: ASP), 55
Ribas, I., Morales, J. C., Jordi, C., Baraffe, I., Chabrier, G., & Gallardo, J. 2008, Mem. Soc. Astron. Ital., 79, 562
Rozyczka, M., Kaluzny, J., Pietrukowicz, P., Pych, W., Mazur, B., Catelan, M., & Thompson, I. B. 2009, Acta Astron., 59, 385
Silva-Valio, A. 2008, ApJ, 683, 179
Strassmeier, K. G. 2009, A&AR, 17, 251
Torres, G, Andersen, J., & Giménez, A. 2010, A&AR, 18, 67
Torres, G., Lacy, C. H., Marschall, L. A., Sheets, H. A., & Mader, J. A. 2006, ApJ, 640, 1018
Torres, G., & Ribas, I. 2002, ApJ, 567, 1140
Washuettl, A., & Strassmeier, K. G. 2001, A&A, 370, 218
Wilson, R. E., & Devinney, E. J. 1971, ApJ, 166, 605